

## CFD Methodology for Simulation of LNG Spills and Rapid Phase Transition (RPT)

Andrei Horvat

### Abstract

Hazards related to transportation and storage of Liquefied Natural Gas (LNG) are widely studied due to an increasing importance of LNG in the overall energy supply. Large scale LNG spills on water are of particular interest as much of LNG transport is conducted by sea. The present work focuses on modelling approaches and their capabilities to predict different phenomena related to LNG spills.

It describes in detail a developed CFD based methodology that is able to simulate the behaviour of LNG spills from their initial release, spreading on the water surface, Rapid Phase Transition (RPT) to subsequent dispersion. The methodology is based on a homogeneous multiphase formulation of the liquid layer and therefore suitable for implementation in most of commercial CFD packages. An LNG release from a process train on a FLNG vessel was used to demonstrate capabilities of the developed approach. A CFD simulation was conducted to calculate volume and distribution of the flammable cloud, and the overpressure generated by an RPT event.

### Keywords

Computational Fluid Dynamics, Liquefied Natural Gas, Rapid Phase Transition, Boiling Regime, Flammability Limit, Cloud Formation, Pressure Load, Hazard Study, Numerical Simulation

## Nomenclature

2D	two-dimensional
3D	three-dimensional
$A$	arbitrary constant
$c$	sonic speed
$c_p$	specific heat capacity at constant pressure
$d$	diameter
$g$	gravitational acceleration
$h$	height or specific enthalpy
$H$	arbitrary function
$j$	mass flow per unit area or mass flux
$\dot{m}$	mass flow rate
$q$	heat flux
$r$	volume fraction
$R$	gas constant
$t$	time
$T$	temperature
$u$	flow speed
$Y$	mass fraction

## Greek letters

$\delta$	small threshold number
$\Delta$	difference
$\gamma$	adiabatic index
$\pi$	Ludolph's number
$\rho$	density

## Subscripts

0	reference value
<i>air</i>	air
<i>amb</i>	ambient gaseous mixture
<i>cont</i>	contact
CH <sub>4</sub> , C <sub>2</sub> H <sub>6</sub> , C <sub>3</sub> H <sub>8</sub>	LNG components
<i>crit</i>	point of vapour film collapse
<i>evap</i>	evaporation
<i>film</i>	film boiling
<i>gas</i>	surrounding gas
<i>i, j</i>	direction indexes
<i>k</i>	chemical species index
<i>layer</i>	liquid layer domain
<i>LNG</i>	liquefied natural gas
<i>max</i>	maximum
<i>min</i>	minimum
<i>pos</i>	positive buoyancy
<i>rel</i>	release
<i>RPT</i>	rapid phase transition
<i>sat</i>	saturation conditions
<i>source</i>	source in the liquid layer domain
<i>super</i>	superheating
<i>water</i>	water

# 1. Introduction

Liquefied Natural Gas (LNG) is becoming an increasingly popular way of transporting otherwise gaseous fuel over large distances. Much of this transport is conducted using LNG ocean carriers. As part of the engineering design and safety assessment process, it is important to understand related hazards due to loss of containment of LNG onto water.

In its liquid form, natural gas is stored below its saturation temperature of  $-162^{\circ}\text{C}$  [1]. In contact with ambient, LNG starts to boil generating a low temperature cloud that is heavier than air. Due to low temperatures, any contact with LNG will cause irreversible tissue damage. Furthermore, strength, ductility and toughness of a ship steel hull will also be affected.

The rate of LNG evaporation depends on the temperature difference between the LNG pool and the water. When the initial film boiling regime collapses, rapid evaporation also known as a Rapid Phase Transition (RPT) event may occur. This will produce a propagating pressure shock front and cause significant structural loads on the ship hull [1]. As the cloud mixes with surrounding air, it becomes flammable. Heated by the ambient, it rises and is finally dispersed by the wind.

There have been a number of studies dedicated to behaviour of LNG spills. Drake et al. [2 & 3] conducted a series of experimental studies on transient boiling of liquid cryogenics on a water surface. The work was partially revisited by Kytömaa and Morse [4]. A summary of experimental data on LNG safety was provided by Cleaver et al. [5]. Their paper presents different safety related issues (e.g. LNG outflow, liquid spread and boil-off, and dense gas dispersion) and acts as a collection of further references. The preceding work by Luketa-Hanin [6] has a similar scope although the effort is extended to modelling of large-scale LNG spills. In both cases, the presented work lacks details that would be directly applicable in an analysis process.

One of the first modelling efforts was presented by Waite et al. [7], who managed to find an analytical solution for an unobstructed spread of LNG on water, water temperature and heat flux to the cryogenic fluid. Probably, the most comprehensive review of analysis techniques was provided by Webber et al. [8]. In much greater detail, Hissong [9] presented an analysis methodology based on time evolution of the LNG pool diameter. A critical review of empirical parameters included in the work provides a very valuable resource for modelling engineers. Nevertheless, the presented model is limited to unobstructed spreading of LNG on water.

A modelling technique based on Computational Fluid Dynamics (CFD) is shown in the paper by Gavelli et al. [10], which focuses on cloud formation and its dispersion. To incorporate the

LNG pool formation, FLACS was used in his later work [11]. Fay [12] and Raj [13] further extended the scope of studies by including fires originated from LNG spills. Similar in scope is the recent series of papers by Sun et al. [14-17], which are focused on LNG vapour dispersion and thermal radiation loading from the resulting pool fire.

The presented short review is just a snapshot of topics, methodologies and techniques that are relevant in risk assessment of LNG spills. These are often applicable to a very constrained set of initial assumptions. Further references will be added later in the text, when specific phenomena are addressed and discussed.

The aim of the current contribution is to present a simulation methodology that has been specifically developed for a mainstream commercial CFD toolset. The discussed models are able to simulate the behaviour of LNG spills from their initial release, spreading on the water surface, Rapid Phase Transition (RPT) to subsequent dispersion. Although individual phases have been addressed before, the robustness of the combined approach is unique.

A complex release scenario studied in a framework of a commercial project is used to illustrate individual phenomena, related modelling assumptions and the model behaviour. The project focused on the behaviour of an LNG spill between the FLNG vessel and the LNG carrier in order to:

- calculate the size of the flammable cloud, and
- determine the resulting overpressure due to an RPT event.

These topics are of particular interest for deterministic risk assessment in the expanding LNG sector.

The paper intentionally uses the project results in a highly selective manner that demonstrates modelling principles, but avoids commercial sensitivity of specific findings. Nevertheless, basic mathematical formulations of fluid dynamics and heat transfer that can be found in any CFD manual may be referenced, but will not be repeated.

## 2. Scenario description

In the analysed scenarios, an LNG carrier is moored alongside an FLNG vessel. Figure 1 shows a general layout of the vessels, their size and the location of the loading arms. Proximity of both vessels importantly determines the shape and the propagation rate of the LNG layer, and the subsequent form of the gaseous cloud.

In the present paper, the results will be presented for the case where a failure in the FLNG process train leads to an LNG release with a mass flow rate of 1020 kg/s and the duration of 76.2 s. The release is at the height of 20 m.

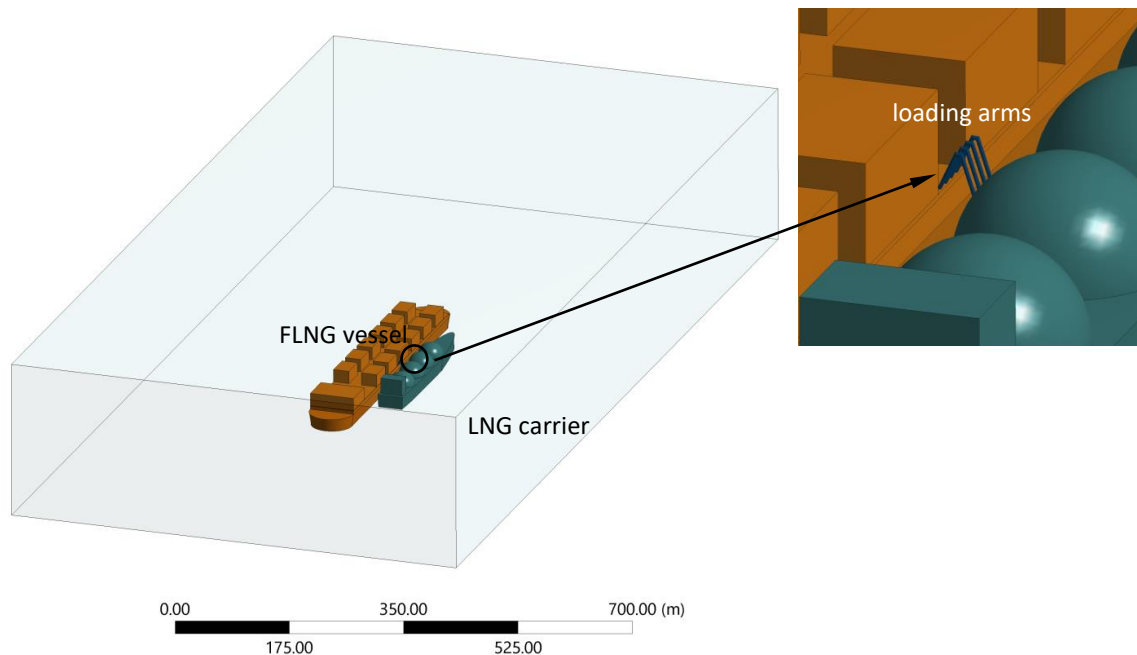


**Figure 1:** Model layout for the LNG spill scenario

The LNG composition was agreed with the client to be a hydrocarbon mixture of the following component mass fractions:  $\text{CH}_4$  - 78.76%,  $\text{C}_2\text{H}_6$  - 12.31% and  $\text{C}_3\text{H}_8$  - 8.93%. The sea and the air temperature were set to 25°C, with the wind speed of 0.5 m/s at the reference height of 50 m.

Simulation of such LNG spill scenario requires an adequate modelling description (i.e. formulation and its numerical implementation) of liquid layer behaviour (dynamics, convective heating, different boiling regimes), compressible effects associated with the RPT phenomenon, and dispersion of gaseous LNG in ambient air. Each section is associated with certain modelling challenges, which will be discussed in detail in two subsequent sections.

### 3. Liquid layer dynamics

Dispersion simulations command the use of large simulation domains to predict cloud behaviour. On the other hand, a liquid layer that serves as a source of gaseous cloud is usually just few millimetres or at most centimetres thick. For that reason, very fine grid spacing is needed to directly resolve the liquid layer. In addition, local liquid surface instabilities do require use of small time-steps, usually below 0.001 s. Both constraints make such CFD simulations prohibitively expensive.

The solution is in two-dimensional approximation of the liquid layer, which is coupled to a larger, three-dimensional ambient domain for dispersion analysis. For that purpose, a commercial CFD code FLACS [18] incorporates a shallow water-based model. When a general purpose CFD codes (e.g. Fluent or CFX) are used, a multiphase formulation is required. Figure 2 show such decomposition of the simulation domain for a simple test case.

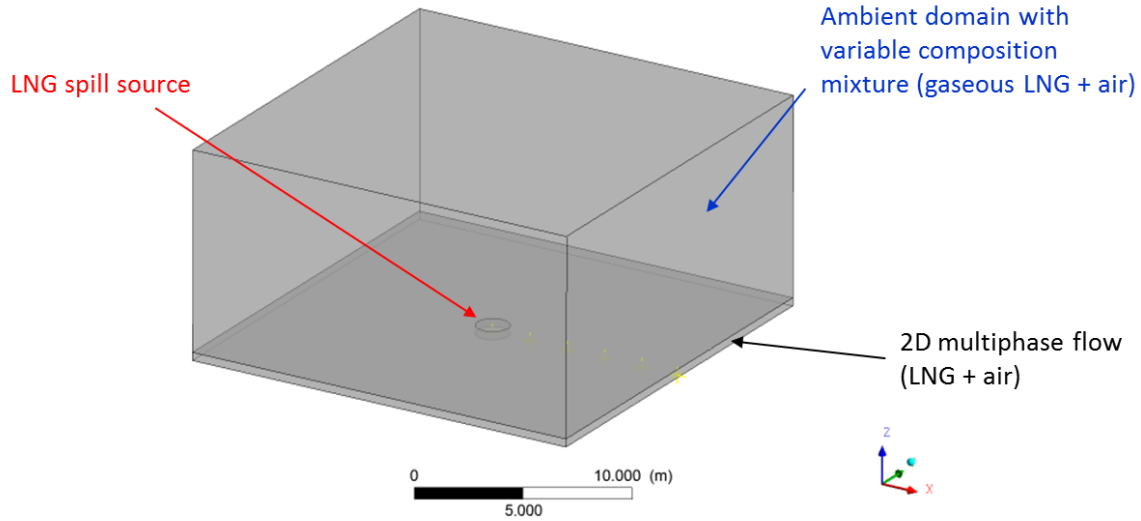


**Figure 2:** Coupling of the 2D liquid layer approximation to the 3D ambient domain for dispersion analysis

The present work is based on a general multiphase formulation of the liquid layer and therefore applicable in most of the general purpose CFD codes. The liquid volume fraction ( $r_{LNG}$ ) substitutes the shallow water formulation using the following relationship:

$$h_{LNG} = r_{LNG} h_{layer} \quad (1)$$

where is  $h_{LNG}$  is the thickness of the LNG layer, and  $h_{layer}$  is the height of the 2D domain. The rest of the layer domain ( $1 - r_{LNG}$ ) is occupied by the entrained air that has the same velocity as the liquid phase. This detail is important in order to preserve continuity of both phases.

### 3.1 Source approximation

The LNG release height ( $h_{rel}$ ) determines the velocity of the liquid at the point of contact with the water:

$$u_{LNG@source} = \sqrt{2gh_{rel}} \quad (2)$$

Higher is the location of the initial release, larger is the liquid velocity at impingement. The main assumption is that kinetic energy of the impinging jet is preserved, and that no addi-

tional surface mixing significantly decreases its flow velocity. This affects the LNG spreading rate, and does represent a conservative assumption. Namely, a higher spreading rate leads to a higher rate of evaporation and, therefore, to a larger cloud of gaseous LNG.

The initial point of a spreading LNG layer can be defined as a volumetric source over certain area with the diameter ( $d_{source}$ ). Although, its diameter is an input parameter, it only defines conditions inside the source volume (Fig. 2):

$$r_{LNG@source} = \frac{\dot{m}_{LNG@rel}}{\rho_{LNG} u_{LNG@source} (0.25\pi d_{source}^2)} \quad (3)$$

where  $\dot{m}_{LNG@rel}$  is the mass flow rate of the release. Outside the source, the liquid volume fraction ( $r_{LNG}$ ) and the related height of the liquid layer ( $h_{LNG}$ ) are independent of the source size and the domain layer thickness ( $h_{layer}$ ). Sun et al. [17] used recently a Gaussian mass flow rate distribution in a similar configuration. Nevertheless, its application yielded no major difference outside the immediate vicinity of the source volume.

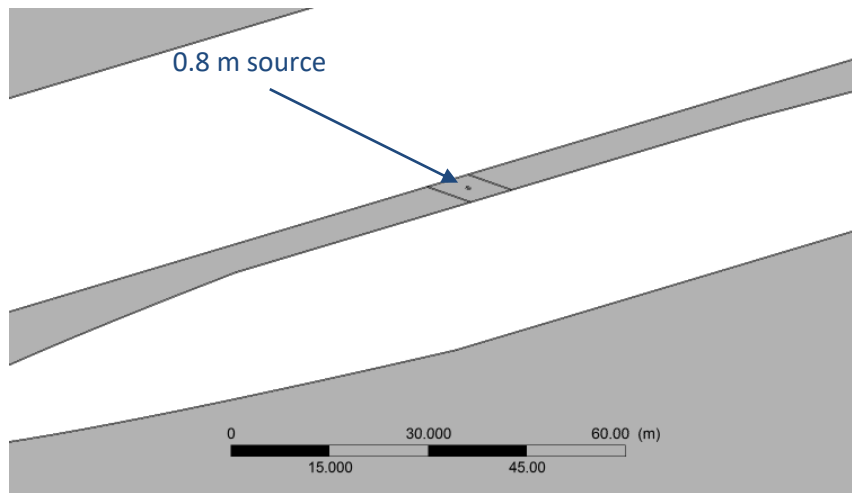


**Figure 3:** Liquid layer source setup

Figure 3 shows the location of the liquid layer source between two vessels. The selected diameter of the source was 0.8 m or twice the reported release diameter ( $d_{source} = 2d_{rel}$ ).

To maintain the same level of kinetic energy, the following equality for the impinging velocity (3) applies:

$$u_{LNG@source} = \frac{\dot{m}_{LNG@rel}}{\rho_{LNG} r_{LNG@source} (0.25\pi d_{source}^2)} = \frac{\dot{m}_{LNG@rel}}{\rho_{LNG} r_{LNG@source} (\pi d_{source} h_{layer})} \quad (4)$$



The side effect of the relation (4) is that it also fully determines the appropriate height of the liquid layer simulation domain:  $h_{layer} = 0.25d_{source}$ .

### 3.2 Spreading of the liquid layer

Spreading rate of the liquid is calculated using a multiphase formulation of the mass transport equation:

$$\partial_t(\rho_{LNG}r_{LNG}) + \partial_i(\rho_{LNG}r_{LNG}u_i) = \frac{\dot{m}_{LNG@rel}}{h_{layer}(0.25\pi d_{source}^2)} \quad (5)$$

where  $r_{LNG}$  is the LNG volume fraction. The source term on the right-hand-side of the equation is applied in the source volume only. It should be noted that a complimentary transport equation for the ambient air volume fraction is also required

$$\partial_t(\rho_{amb}r_{amb}) + \partial_i(\rho_{amb}r_{amb}u_i) = \frac{\dot{m}_{LNG@rel}}{h_{layer}(0.25\pi d_{source}^2)} \left( \frac{\rho_{amb}}{\rho_{LNG}} \right) \left( \frac{1 - r_{LNG@source}}{r_{LNG@source}} \right) \quad (6)$$

to maintain the volume fraction ratio and the related LNG layer thickness.

For the presented model, the homogenous multi-phase formulation was selected. This brought an additional resistance to the liquid layer dynamics, but the conducted tests did not produce large differences in comparison to the heterogeneous model.

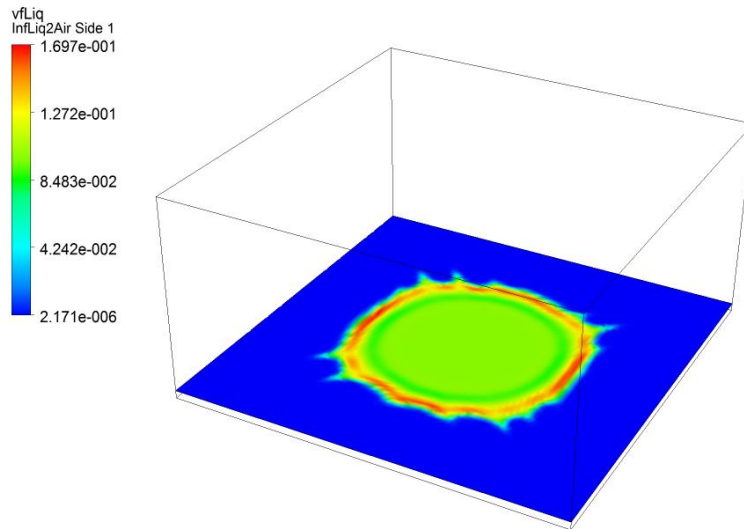


**Figure 4:** Liquid volume fraction distribution for the model test case  
20s from the start of the release

Figure 4 presents the liquid volume fraction distribution 20s from the start of the release for one of such tests. Higher volume fraction near the progressing front clearly shows the hydraulic jump and the initial jet atomisation.

### 3.3 Domain interface exchange

The liquid layer domain is coupled to the ambient domain through source terms. On the liquid side, these are volumetric source terms to model the LNG phase change and to maintain the 2D approximation. For the ambient domain, the source terms are associated with the interface surface only.

The mass exchange between the liquid layer and the ambient domain was modelled as an asymmetric process. Only the mass flow associated with the LNG boiling was allowed to appear at the ambient side in exactly the same extent as it was removed from the liquid layer domain:

$$\begin{aligned}\partial_t(\rho_{LNG}r_{LNG}) + \partial_i(\rho_{LNG}r_{LNG}u_i) &= \dots - \frac{j_{evap}}{h_{layer}} \\ \partial_t(\rho_{amb}Y_k) + \partial_i(\rho_{amb}Y_k u_i) &= \dots + Y_k \frac{j_{evap}}{h_{layer}}\end{aligned}\quad (7)$$

where  $Y_k$  are mass fractions of the gaseous LNG,  $\rho_{amb}$  is the density in the ambient domain, and  $j_{evap}$  is the mass flux associated with LNG evaporation.

It is important to repeat that the gaseous LNG was modelled as a fixed composition mixture of air, methane ( $CH_4$ ), ethane ( $C_2H_6$ ) and butane ( $C_3H_8$ ). Therefore, the ambient domain density is defined as:

$$\frac{1}{\rho_{amb}} = \frac{Y_{air}}{\rho_{air}} + \frac{Y_{CH_4}}{\rho_{CH_4}} + \frac{Y_{C_2H_6}}{\rho_{C_2H_6}} + \frac{Y_{C_3H_8}}{\rho_{C_3H_8}} \quad (8)$$

Because of the liquid layer domain two-dimensionality, the flow conditions are much more sensitive to any mass source or sink than in the ambient domain. For that reason, the volume outflow rate associated with LNG boiling in the liquid domain has to be compensated with an equal volume inflow rate of the surrounding ambient air. Thus, the following source term was added to the transport equation for the ambient air volume fraction in the liquid domain:

$$\partial_t(\rho_{amb}r_{amb}) + \partial_i(\rho_{amb}r_{amb}u_i) = \dots + \frac{j_{evap}}{h_{layer}} \left( \frac{\rho_{amb}}{\rho_{LNG}} \right) \quad (9)$$

As the liquid spreads, it supplants the gaseous phase around the domain. Because the domain is closed in the vertical direction, any movement of the gaseous phase has also a profound effect on the shape of the liquid phase. Such behaviour is a modelling artefact due to two-dimensionality of the liquid layer modelling approach. In reality, the ambient air is exchanged (or entrained) in the vertical direction, perpendicular to the liquid layer.

To introduce the vertical exchange of ambient air to the liquid layer domain, additional source terms were added to the momentum transport equation for the gaseous phase:

$$\partial_t(\rho_{amb}r_{amb}u_j) + \partial_i u_i(\rho_{amb}r_{amb}u_j) = \dots - (\rho_{amb}r_{amb}u_j)\frac{u_i}{h_{layer}} + (\rho_{amb}r_{amb}u_j)\frac{u_0}{h_{layer}} \quad (10)$$

The first term on the right hand side of Eq. (10) removes the accelerated gaseous flow from the simulation domain, whereas the second term replaces it with the same amount of zero velocity ( $u_0 = 0$  m/s) ambient air.

It is important to note that the additional source terms for modelling the entrainment process are only required due to the multiphase formulation that includes the liquid as well as the gaseous phase in the two-dimensional layer domain. If the utilized CFD code allows modelling of the liquid phase without the feedback effects from the gaseous phase (e.g. shallow water [18] or volume-of-fluid [19] based models) such additions are not required.

Figure 5 shows the results of a model test using a constant LNG evaporation mass flux ( $j_{evap}$ ) of 0.2 kg/m<sup>2</sup>s. The selected value complies with observations described in [4 & 9], although the LNG evaporation rate will be addressed in great detail later in the text.

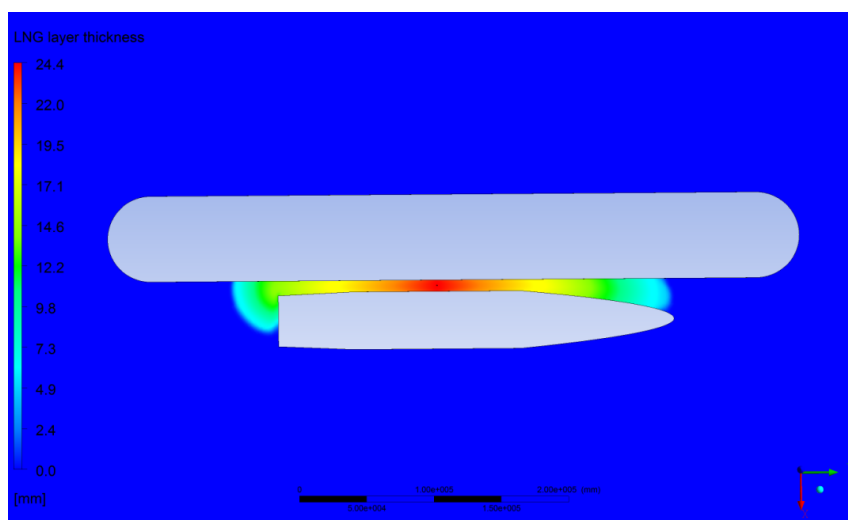


**Figure 5:** Shape of the spreading LNG layer between 2 vessels 80s from the start of the release

The test was performed for the same release parameters as described in Section 2. The thickness of the LNG layer, which is shown 80s from the start of the release, is the highest near the source. It uniformly decreases toward the progressing front due to the constant evaporation mass flux used in the model.

#### 4. Boiling regimes and RPT

The saturation temperature of LNG at atmospheric conditions is  $-162^{\circ}\text{C}$  (or 111 K). This means that in contact with water it starts to boil. There has been a lot of research in different LNG boiling regimes mostly to accurately determine the associated evaporation mass flux. The values between  $0.02$  and  $0.3 \text{ kg/m}^2\text{s}$  have been recorded by different research groups [4 & 9].

In the initial tests of the presented work, a single value of  $0.2 \text{ kg/m}^2\text{s}$  was selected for the LNG evaporation mass flux. Such coarse approximation cannot be used to model the Rapid Phase Transition (RPT) phenomenon. To capture RPT, different boiling regimes and the associated evaporation mass flux have to be introduced in the modelling procedure.

Melhem et al. [1] stated that the RPT is the result of the LNG layer superheating. When the maximum superheating limit (i.e. the spinodal state) is reached, the accumulated thermal energy is released instantaneously by a rapid phase change from liquid to gas. As a result, a pressure wave is formed that propagates through the ambient air. A sketch in Fig. 6 shows the LNG temperature - enthalpy diagram with marked initial saturation conditions, superheating, RPT and further heating of the gaseous LNG.

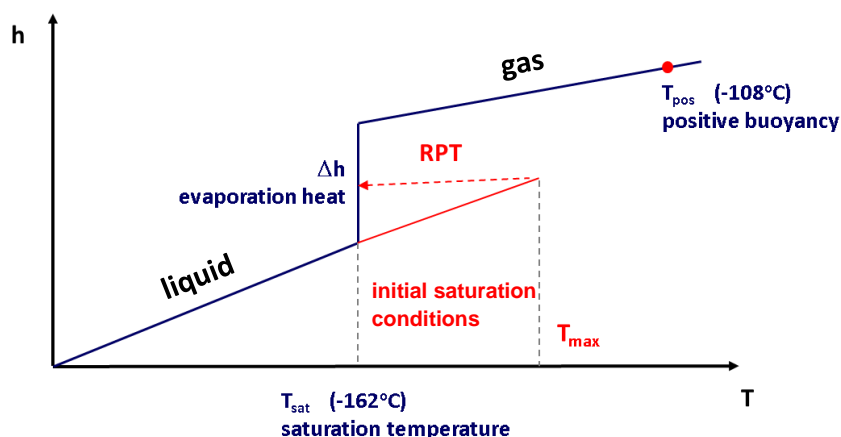


**Figure 6:** Sketch of the LNG temperature - enthalpy diagram

The phase transition in Fig. 6 does not reveal different boiling regimes with the associated evaporation mass fluxes. A boiling diagram in Fig. 7 relates the temperature difference between the surface and the LNG layer ( $T_{water} - T_{LNG}$ ) with the resulting heat flux to the LNG layer ( $q_{evap}$ ). It is reconstructed from diagrams found in [1 & 20] although in both instances the work is based on much older data [21].

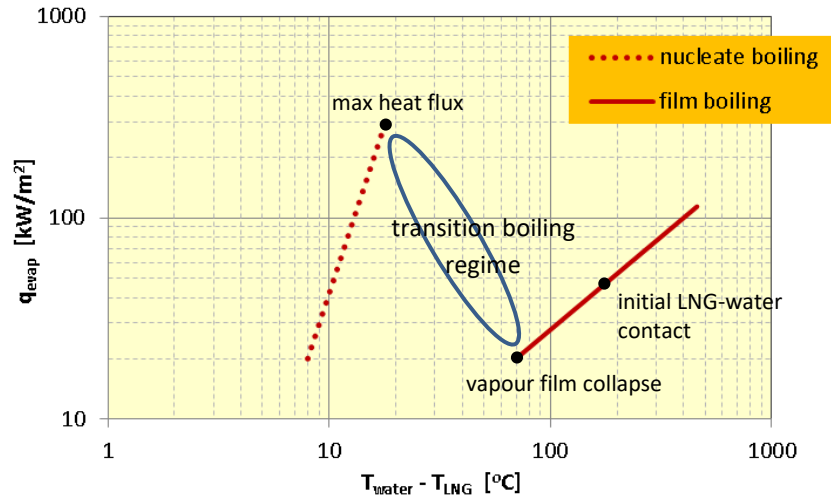


**Figure 7:** LNG boiling curve

Once the heat flux  $q_{evap}$  is calculated, the associated evaporation mass flux is simply

$$j_{evap} = \frac{q_{evap}}{\Delta h_{evap}} \quad (11)$$

where  $\Delta h_{evap}$  is the LNG latent heat of evaporation. In the analysis, an average value of 641.3 kJ/kg was calculated based on the review study [9].

The water temperature of interest was 25°C resulting in a temperature difference of 187°C at the LNG-water contact. Such high temperature difference facilitates film boiling. The temperature difference starts to decrease as the water surface cools down and freezes.

#### 4.1 Film boiling regime

Thermal state of the water surface is not directly included in the current model, which means that it needs to be approximated by an empirical correlation.

The evaporation mass flux decreases with the contact time as discussed in [22]. Its maximum  $j_{max}$  is at the point of the initial LNG jet impingement, when direct contact between LNG and water still exists. This brings additional complexity as the local contact time needs to be tracked and recorded during the CFD simulation.

To track the contact time, the following equation was used:

$$\partial_t t_{cont} = H(r_{LNG}), \quad \text{where } H(r_{LNG}) = \begin{cases} 1, & r_{LNG} > \delta \\ 0, & r_{LNG} \leq \delta \end{cases} \quad (12)$$

and where  $\delta$  is a small threshold number.

Based on the experimental data [22] for a similar LNG composition, the following linear function was implemented for the evaporation mass flux in the film boiling regime:

$$j_{film} = j_{max} - At_{cont}, \quad \text{where } j_{max} = 0.38 \frac{kg}{m^2s} \text{ and } A = 0.015 \frac{kg}{m^2s}. \quad (13)$$

Figure 8 shows the local distribution of the evaporation mass flux due to the contact time dependence.

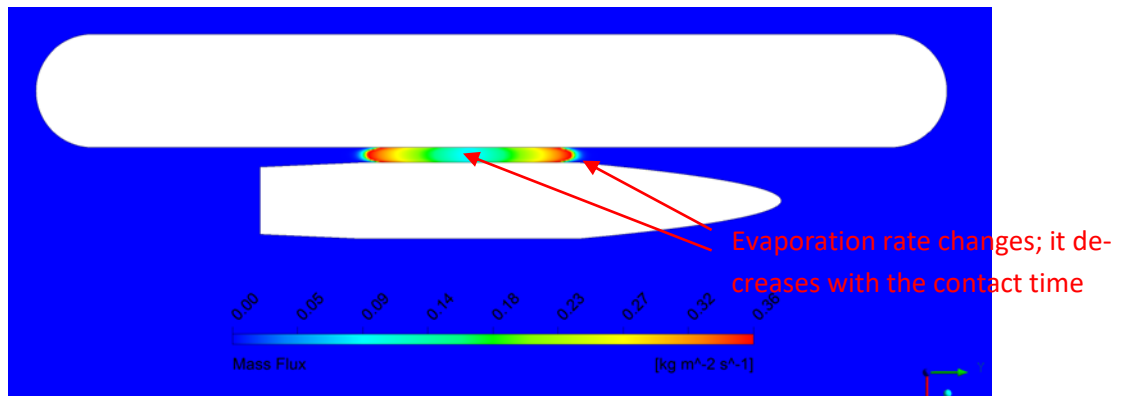


**Figure 8:** Contact time simulation test - evaporation mass flux between the vessels after 20 s

#### 4.2 Transition boiling regime

The vapour film collapses when the temperature difference ( $T_{water} - T_{LNG}$ ) decreases to approximately 70 - 80°C (Fig. 7). At that point, the LNG comes into a direct contact with the water surface. As the LNG layer is at its saturation temperature, the lowest temperature difference is essentially determined by the minimum surface temperature  $T_{water}$ .

Combining the film boiling part of the curve in Fig. 7:

$$q_{film} = q_0((T_{water} - T_{sat})/1^\circ C)^{0.923389}, \quad \text{where } q_0 = 395.629 \frac{W}{m^2} \quad (14)$$

and the evaporation mass flux dependence from the contact time (13) allows us to determine the contact time ( $t_{crit}$ ) needed to reach the LNG boiling crises based on the minimum temperature requirement:

$$t_{crit} = \frac{1}{A} \left( j_{max} - \frac{q_0}{\Delta h_{evap}} (\Delta T_{min}/1^\circ\text{C})^{0.923389} \right), \text{ where } \Delta T_{min} = 80^\circ\text{C} \quad (15)$$

When the local contact time exceeds  $t_{crit}$ , the heat flux from water to the LNG layer increases to  $q_{max}$ . At present, this was set to 300 kW/m<sup>2</sup> although some authors [7 & 20] reported even higher values.

This transition between the film and the nucleate boiling regime is quick, but only a part of the available heat transfer to LNG can be continuously utilized in the LNG evaporation. If  $j_{max}$  (13) is the maximum evaporation mass flux that arises from the direct contact between two phases, then the difference

$$q_{max} - \Delta h_{evap} j_{max}, \text{ where } q_{max} = 300 \frac{\text{kW}}{\text{m}^2} \text{ and } j_{max} = 0.38 \frac{\text{kg}}{\text{m}^2\text{s}} \quad (16)$$

is used for the LNG layer superheating. This causes the temperature of the liquid layer to increase, eventually leading to an RPT event.

Figure 9 shows the local distribution of the evaporation mass flux when the transition boiling model with the liquid layer superheating is included in the CFD simulation.

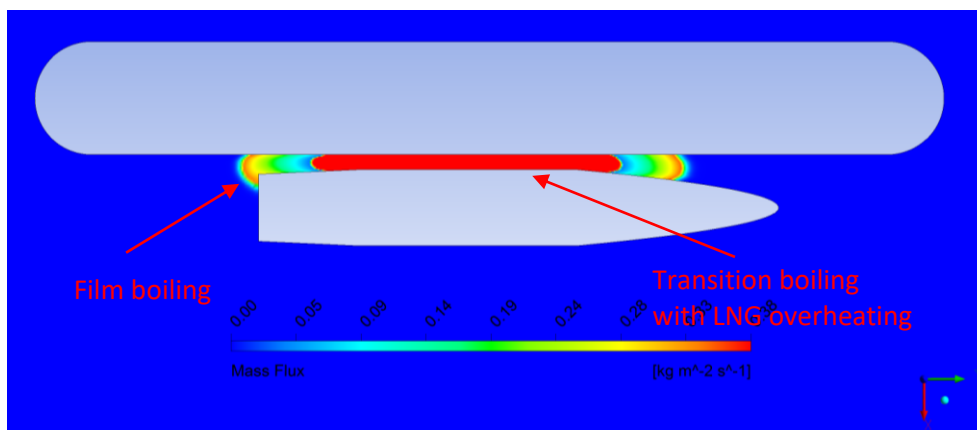


**Figure 9:** Transition boiling simulation test - evaporation mass flux between the vessels after 56 s

### 4.3 Rapid phase transition

When the LNG liquid layer reaches the maximum superheating temperature ( $T_{max}$ ), it triggers an RPT event. In the present model,  $T_{max}$  was set to 191 K as proposed by Melhem et al. [1] for a similar LNG composition.

During the RPT event the sensible heat accumulated in the form of LNG superheating is released causing rapid evaporation:

$$\begin{aligned} \partial_t(\rho_{LNG}r_{LNG}) + \partial_i(\rho_{LNG}r_{LNG}u_i) &= \dots - \frac{j_{RPT}}{h_{layer}} \\ \partial_t(\rho_{LNG}r_{LNG}h_{super}) + \partial_i(\rho_{LNG}r_{LNG}u_i h_{super}) &= \dots - \frac{j_{RPT}}{h_{layer}} (\Delta h_{evap}) \end{aligned} \quad (17)$$

where  $h_{super} = c_p(T_{LNG} - T_{sat})$ . The process finishes when  $h_{super}$  decreases to zero.

The resulting evaporation mass flux is high, but not infinite. It has to be limited by the sonic speed of the surrounding gas:

$$j_{RPT} = \rho_{gas}c_{gas} \quad \text{where } c_{gas} = \sqrt{\gamma RT_{sat}} \quad (18)$$

Although the composition changes as the LNG evaporates and mixes with the surrounding ambient air, the material properties of gaseous LNG were used to determine  $j_{RPT}$ . Figure 10 shows the evaporation mass flux ( $j_{RPT}$ ) during the simulated RPT event.

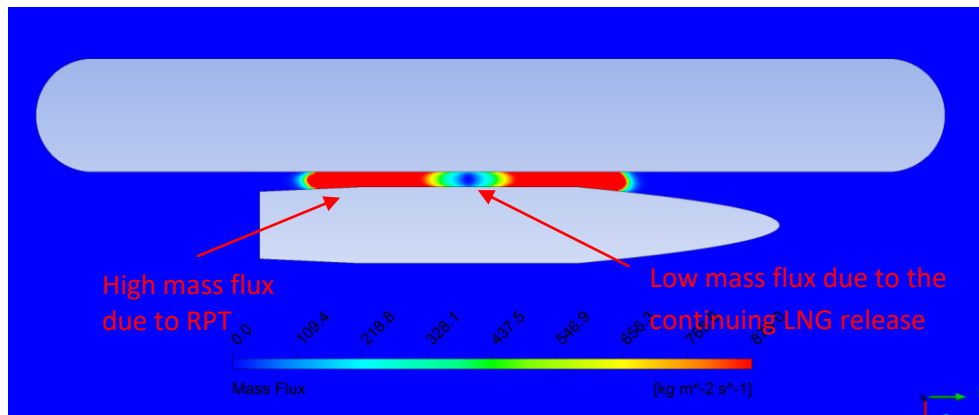


**Figure 10:** RPT simulation test - evaporation mass flux between the vessels after 55.4 s



#### 4.4 Nucleate boiling

Once the thermal energy associated with LNG superheating ( $h_{super}$ ) decreases to zero, the RPT event also concludes. It is assumed that the remaining LNG is well mixed with water and, therefore, evaporation continues in the nucleate boiling regime.

Due to a low temperature difference between the LNG and water, a direct contact between LNG and water becomes possible. For that reason, the maximum evaporation mass flux ( $j_{max}$ ) can be assumed [20].

### 5. Dispersion

The evaporation mass flux is transferred from the liquid layer domain to the gaseous, ambient domain using the source terms as discussed in Section 3.3:

$$\partial_t(\rho_{amb}Y_k) + \partial_i(\rho_{amb}Y_k u_i) = \dots + Y_k \frac{j_{evap}}{h_{layer}} \quad (19)$$

where  $Y_k$  are mass fractions of the gaseous LNG. The imposed wind velocity field disperses generated gaseous LNG. Figure 11 shows the initial velocity field for the imposed wind speed of 0.5 m/s.

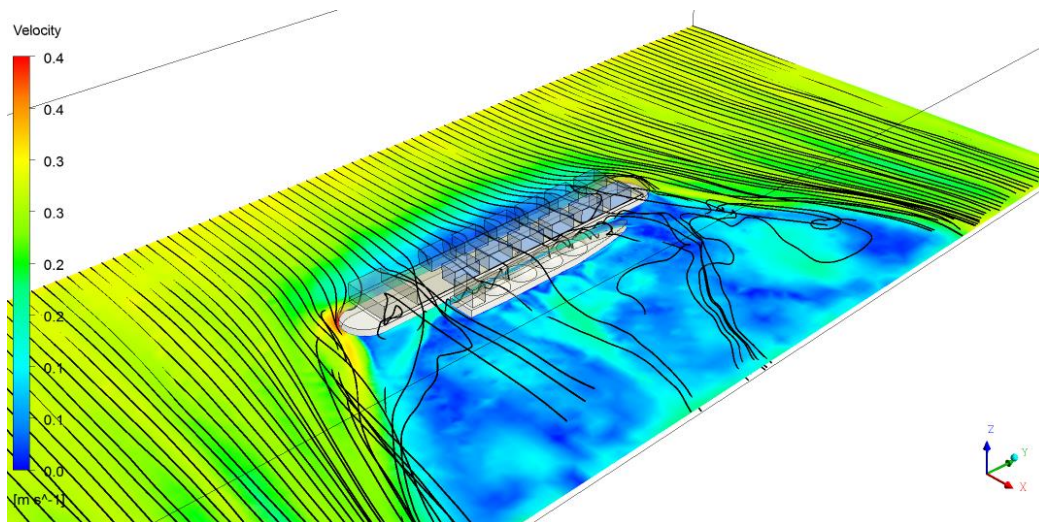


**Figure 11:** Imposed initial velocity field due to cross-wind

It has to be noted that the dispersion of the gaseous LNG cloud mostly depends on its buoyancy. At the beginning the gaseous LNG is at the saturation temperature ( $-162^{\circ}\text{C}$ ) and, therefore, it is negatively buoyant. Due to its higher density it freely flows above the water surface (Fig. 12).

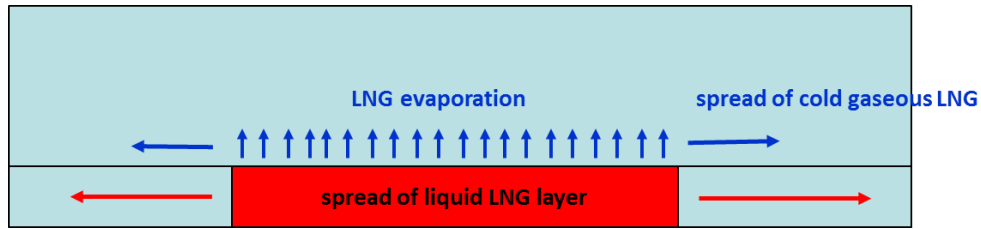


**Figure 12:** Spread of gaseous LNG due to negative buoyancy

The cloud needs to heat-up above  $-108^{\circ}\text{C}$  to become positively buoyant. It is buoyancy that lifts it up from the water surface and strongly enhances its dispersion. The heating process is controlled by mixing with the surrounding air. Figure 13 shows the dispersing LNG cloud after 320 s.

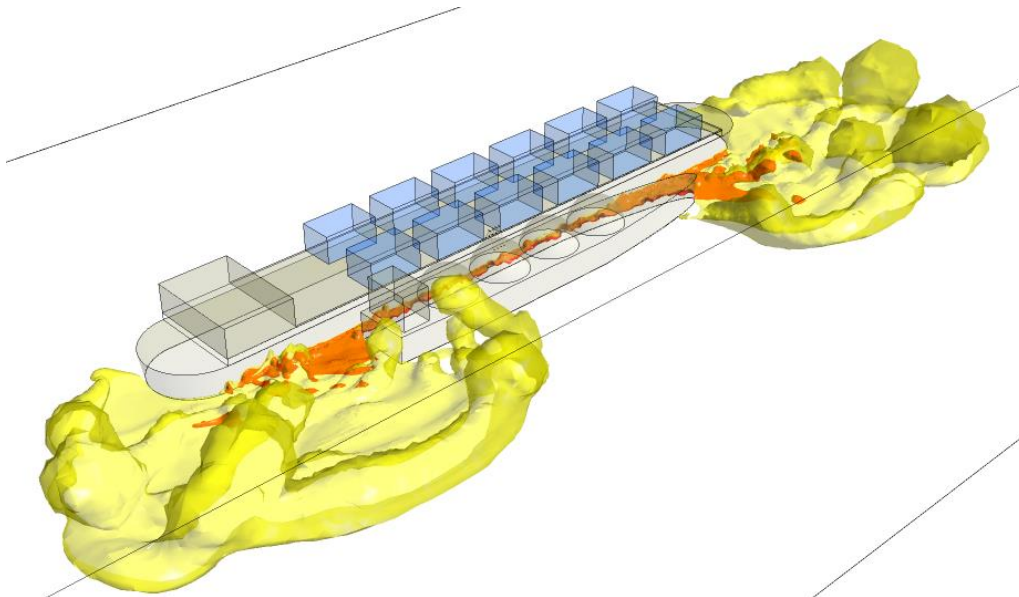


**Figure 13:** Dispersing cloud of gaseous LNG (1 and 10% mass fraction isosurfaces) after 320 s

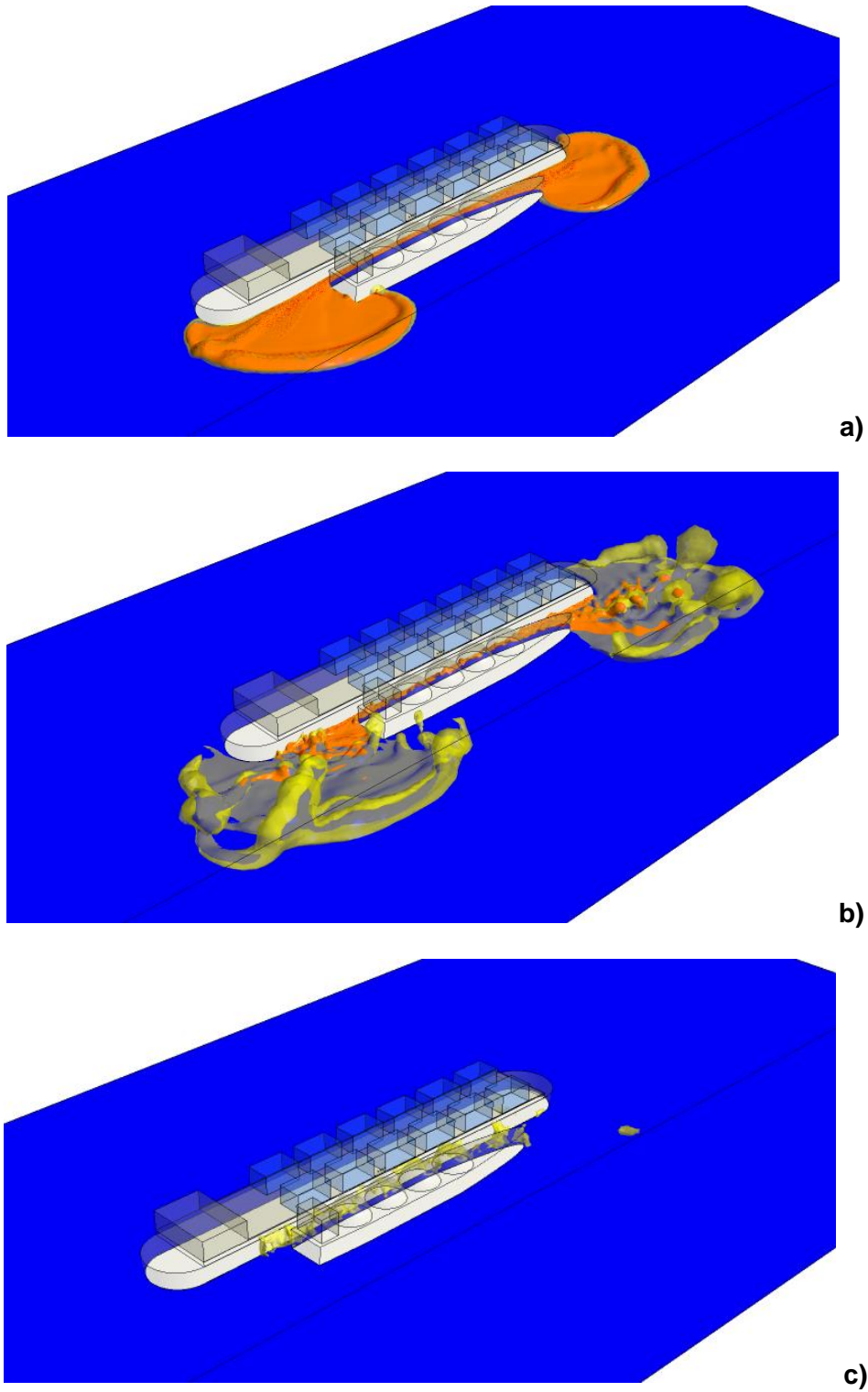
## 6. CFD simulation results and discussion

The CFD model was prepared in the ANSYS CFX simulation environment [23] mostly because of simplicity to add different model extensions. Although a number of different scenarios were analysed, the results will be presented only for the process train release case that was fully defined in Section 2.

Two main analysis objectives are discussed and visualised: a) volume of the flammable cloud and its distribution, and b) overpressure approximation due to RPT.

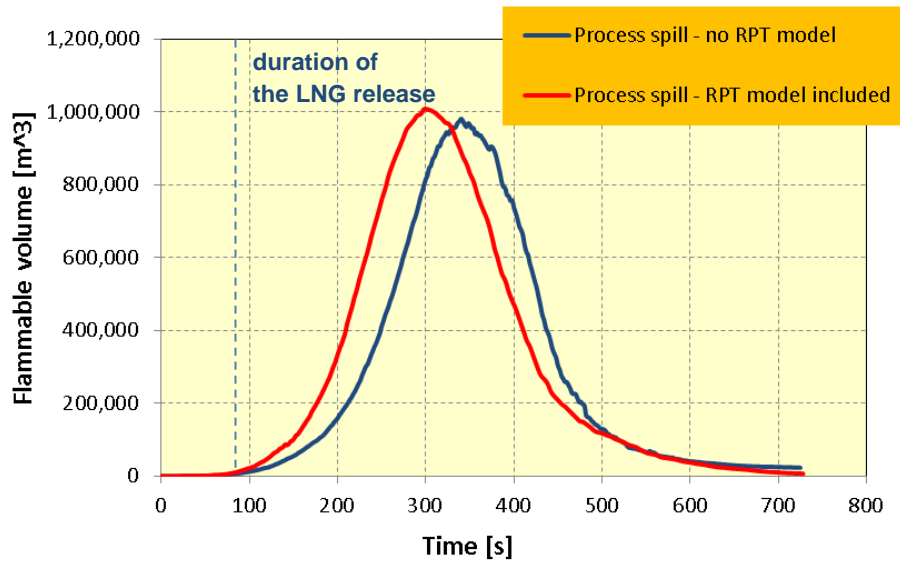
## 6.1 Flammability limits and volume of the cloud

Figure 14 shows the development of the gaseous cloud. Two isosurfaces illustrate volume fraction of the lower (4.5%) and the upper (15%) flammability limit at 25°C.



**Figure 14:** Lower and upper flammability limit after 160 s (a), 320 s (b) and 640 s (c)

The CFD analysis shows that the gaseous LNG remains present between both vessels long after it has dispersed from more wind-exposed areas. This is due to negative buoyancy of the gaseous LNG and the time required for the cloud lift-off, which is mostly independent from the duration of the initial spill. The diagram in Fig. 15 shows the integrated flammable volume for two analysed cases and confirms these observations.



**Figure 15:** Time variation of the gaseous LNG flammable volume

## 6.2 Overpressure approximation

The extent of an RPT event is constrained by the LNG layer superheating. As such, it does not involve a significant amount of LNG. Therefore, its effect on the dispersion process of the gaseous LNG is limited. Figure 15 shows that the time variation of the flammable volume is practically unchanged by the RPT event.

The most important manifestation of the RPT event is a pressure wave that is formed. It propagates through the ambient domain with the sonic speed. Figure 16 shows the pressure wave after 55.1s and Fig. 17 again after 55.27s.

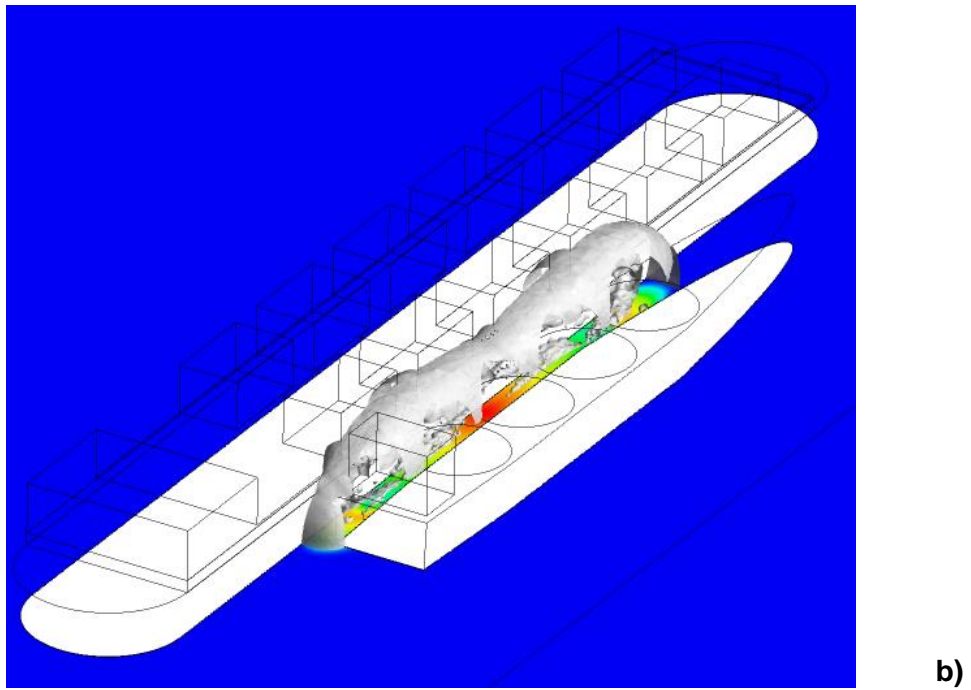
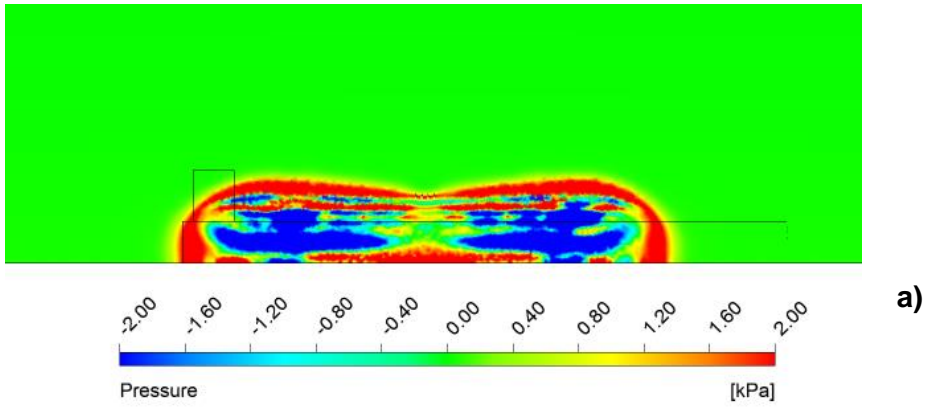


**Figure 16:** Pressure wave after the RPT event (55.1 s):  
 (a) overpressure contour plot, (b) 400 Pa isosurface

The overpressure is high at the beginning, close to the LNG layer, and decreases with radial expansion of the pressure wave. Figures 16 and 17 also show that the shape of the propagating wave is importantly influenced by both vessels. They represent an obstruction, which leads to local pressure wave reflections.

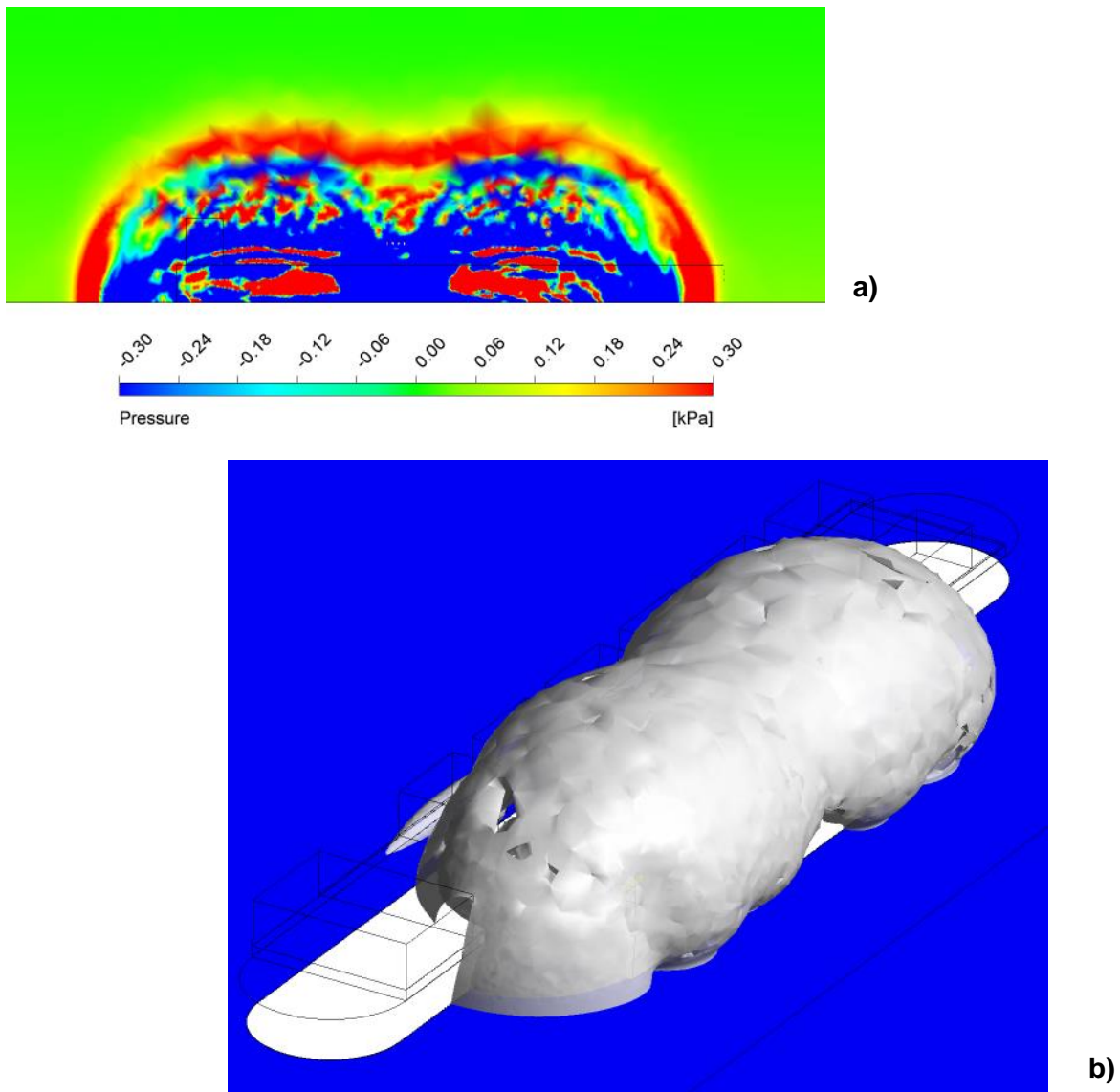


**Figure 17:** Pressure wave after the RPT event (55.27 s):  
 (a) overpressure contour plot, (b) 200 Pa isosurface

The time variation of maximum overpressure is presented in Fig. 18. It shows that the maximum overpressure exceeds 110 kPa. Although similar pressure peak values have also been reported, larger variations can be found due to differences in experimental conditions [1].

The pressure peaks occur near the water surface, where the temperatures are close to the LNG saturation temperature of  $-162^{\circ}\text{C}$ . This combination of high pressures and extremely low temperatures does pose a significant risk of structural failure.

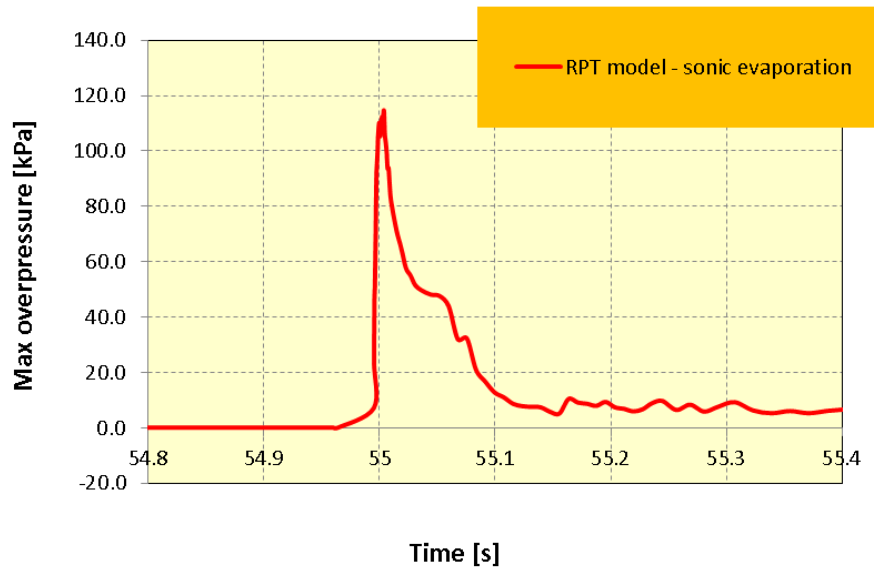


**Figure 18:** Time variation of the maximum overpressure during the RPT event

## 7. Further challenges and conclusions

The paper presents a CFD modelling approach to simulate the behaviour of LNG spills from their initial release, spreading on the water surface, rapid phase transition to subsequent dispersion.

- The described approach is generic and can be used in most of the available CFD codes that include multiphase flow capabilities.
- The author is well aware that many modelling simplifications especially in formulating the effects of different boiling regimes were utilized by using available sources discriminatorily.
- In most of the reviewed cases, the modelling relies on a single source for the boiling curve definition [21]. Until more complete data is available, this will remain the weakest point in any modelling approach.
- The energy transport equation was not used in modelling the LNG liquid layer to avoid the definition of the heat transfer between the water and the liquid layer. Such definition would have to involve or at least quantify the effects of ice formation and its thickness, state of the surface and any convective mixing.

- The CFD simulation results that are included in the paper demonstrate the capability of the developed methodology. They are related to a failure in the FLNG process train that leads to an LNG release in a highly constrained space between two vessels.
- The analysis methodology allows to estimate the size and distribution of the flammable cloud generated by the LNG spill. The simulation results identified an important behaviour. Due to negative buoyancy, the flammable cloud initially spreads in the horizontal directions. For that reason, it does not reach the process decks, which significantly lowers the fire related hazard.
- The overpressure prediction due to an RPT event shows that the maximum exceeds 110 kPa. Such high pressure in combination with low temperatures (-162°C) may lead to a structural failure of the vessel hull. It is important to emphasize that further parametric studies are needed to determine the sensitivity of the RPT induced pressure peaks to the size of LNG release, speed of evaporation and ambient temperature.



## References

1. G.A. Melhem, S. Saraf & H. Ozog, Understand LNG Rapid Phase Transitions (RPT), io-Mosaic Corporation, 2006.
2. E.M. Drake, A.A. Jeje & R.C. Reid, Transient boiling of liquefied cryogens on a water surface: I. Nitrogen, methane and ethane, *Int. J. Heat Mass Transfer*, 1975, Vol. 18, pp. 1361-1368.
3. E.M. Drake, A.A. Jeje & R.C. Reid, Transient boiling of liquefied cryogens on a water surface: II. Light hydrocarbon mixture, *Int. J. Heat Mass Transfer*, 1975, Vol. 18, pp. 1369-1375.
4. H.K. Kytömaa and T.L. Morse, Variations in the evaporation rate of a cryogenic liquid on a water surface, 2010 Int. Sym., Beyond Regulatory Compliance, Making Safety Second Nature, Oct. 26-28, 2010, Hilton College Station Conference Center, College Station, Texas, USA.
5. P. Cleaver, M. Johnson & B. Ho, A summary of some experimental data on LNG safety, *J. Hazardous Materials*, 2007, Vol. 140, pp. 429-438.
6. A. Luketa-Hanlin, A review of large-scale LNG spills: Experiments and modeling, *J. Hazardous Materials*, 2006, Vol. A132, pp. 119-140.
7. P.J. Waite, R.J. Whitehouse, E.B. Winn & W.A. Wakeham, The spread and vaporisation of cryogenic liquids on water, *J. Hazardous Materials*, 1983, Vol. 3, pp. 165-184.
8. D.M. Webber, S.E. Grant, M.J. Ivings, S.F. Jagger, LNG source term models for hazard analysis - A review of the state-of-the-art and an approach to model assessment, RR789 Health and Safety Laboratory, 2010
9. D.W. Hissong, Keys to modeling LNG spills on water, *J. Hazardous Materials*, 2007, Vol. 140, pp. 465-477.
10. F. Gavelli, E. Bullister & H. Kytömaa, Application of CFD (Fluent) to LNG spills into geometrically complex environments, *J. Hazardous Materials*, 2008, Vol. 159, pp. 158-168.
11. F. Gavelli, S.G. Davis & O.R. Hansen, A unified model for LNG pool spread and vapor dispersion: Is wind scooping really a factor? American Institute of Chemical Engineers, 2010 Spring Meeting, 10th Topical Conference on Gas Utilization, March 24, 2010, San Antonio, Texas, USA.

12. J.A. Fay, Model of spills and fires from LNG and oil tankers, *J. Hazardous Materials*, 2003, B96, pp. 171-188.
13. P.K. Raj, LNG fires: a review of experimental results, models and hazard prediction challenges, *J. Hazardous Materials*, 2007, 140, pp. 444-464.
14. B. Sun, R.P. Utikar, V.K. Pareek, K. Guo, Computational fluid dynamics analysis of liquefied natural gas dispersion for risk assessment strategies. *J. Loss Prev. Process Ind.*, 2013, 26, pp. 117–128.
15. B. Sun, K. Guo, V.K. Pareek, Computational fluid dynamics simulation of LNG pool fire radiation for hazard analysis, *J. Loss Prev. Process Ind.*, 2014, 29, pp. 92–102.
16. B. Sun, K. Guo, V.K. Pareek, Dynamic simulation of hazard analysis of radiations from LNG pool fire, *J. Loss Prev. Process Ind.*, 2015, 35, pp. 200–210.
17. B. Sun, K. Guo, V.K. Pareek, Hazardous consequence dynamic simulation of LNG spill on water for ship-to-ship bunkering, *Process Safety and Environmental Protection*, 2017, 107, pp. 402–413.
18. O.R. Hansen, M. Ichard & S.G. Davis, Validation of FLACS for vapor dispersion from LNG Spills: Model evaluation protocol, 12th Annual Symposium, Mary Kay O'Connor Process Safety Center, October 27-28, 2009, Texas A&M University, College Station, Texas, USA, pp. 712-743.
19. Ansys Inc, *Fluent Rel. 18.0, User Manual*, Section 17.3 - Volume of Fluid (VOF) model theory.
20. G.-M. Wuersig, J. Gaughan, B. Scholz, L. Sannes, S. Kabelac, A. Leder, Effects of enveloping pool fires on LNG tank containment systems, May 25 – 28, 2009, GasTech, Abu-Dhabi.
21. C.T. Sciance, C.P. Colver, C.M. Sliepcevich, Pool boiling of methane between atmospheric pressure and the critical pressure, *Advances in Cryogenic Engineering*, Vol. 12, Jan. 1967.
22. Panel on Liquefied Natural Gas Safety Evaluation, *Safety Aspects of Liquefied Natural Gas in the Marine Environment*, Report NMAB-354, United States Coast Guard, 1980, p. 274.
23. [www.ansys.com/products/fluids/ansys-cfx](http://www.ansys.com/products/fluids/ansys-cfx), accessed 2017/04/13.